Water Research 234 (2023) 119812

Contents lists available at ScienceDirect

Water Research

journal homepage: www.elsevier.com/locate/watres

Spatiotemporal response of dissolved organic matter diversity to natural and anthropogenic forces along the whole mainstream of the Yangtze River

Shuaidong Li [a,f], Lize Meng [a], Chu Zhao [a], Yu Gu [a], Robert G.M. Spencer [e], Xosé Antón Álvarez–Salgado [f], Anne M. Kellerman [e], Amy M. McKenna [g], Tao Huang [a,b,c,d], Hao Yang [a,b,c,d], Changchun Huang [a,b,c,d,*]

[a] School of Geography, Nanjing Normal University, Nanjing 210023, China
[b] Jiangsu Center for Collaborative Innovation in Geographical Information Resource Development and Application, Nanjing Normal University, Nanjing 210023, China
[c] Key Laboratory of Virtual Geographic Environment (Nanjing Normal University), Ministry of Education, Nanjing 210023, China
[d] State Key Laboratory Cultivation Base of Geographical Environment Evolution (Jiangsu Province), Nanjing 210023, China
[e] Department of Earth, Ocean and Atmospheric Science, Florida State University, Tallahassee, FL 32306, USA
[f] Organic Geochemistry Lab, Instituto de Investigacións Mariñas (IIM), Consejo Superior de Investigaciones Científicas (CSIC), Vigo 36208, Spain
[g] National High Magnetic Field Laboratory, Florida State University, Tallahassee, FL 32310, USA

ARTICLE INFO

Keywords:
Dissolved organic matter
Optical properties
Molecular composition
Driving factors
Yangtze river

ABSTRACT

The Yangtze River, the largest river in Asia, plays a crucial role in linking continental and oceanic ecosystems. However, the impact of natural and anthropogenic disturbances on composition and transformation of dissolved organic matter (DOM) during long-distance transport and seasonal cycle is not fully understood. By using a combination of elemental, isotopic and optical techniques, as well as Fourier-transform ion cyclotron resonance mass spectrometry (FT-ICR MS), we investigated DOM abundance and composition along the whole mainstream at highly spatial resolution in the dry and early wet seasons. Our findings showed that the concentration and flux of dissolved organic carbon (DOC) in the Yangtze River was much lower compared with other worldwide larger rivers. The distribution of $\delta^{13}C_{DOC}$ and higher abundance of humic-like fluorescent component and highly unsaturated and phenolics (HUPs) compound reflected a prominent contribution of allochthonous DOM. Further optical and molecular analysis revealed humic-like fluorescent components were coupled with CHO molecules and HUPs compound with higher aromatic, unsaturated, molecular weight and stable characteristics between upstream and midstream reaches. With increasing agricultural and urban land downstream, there were more heteroatomic formulae and labile aliphatic and protein-like compounds which were derived from human activities and in situ primary production. Meanwhile, DOM gradually accumulates with slow water flow and additional autochthonous organics. Weaker solar radiation and water dilution during the dry/cold season favours highly aromatic, unsaturated and oxygenated DOM compositions. Conversely, higher discharge during the wet/warm season diluted the terrestrial DOM, but warm temperatures could promote phytoplankton growth that releases labile aliphatic and protein-like DOM. Besides, chemical sulfurization, hydrogenation and oxygenation were found during molecular cycling processes. Our research emphasizes the active response of riverine DOM to natural and anthropogenic controls, and provides a valuable preliminary background to better understand the biogeochemical cycling of DOM in a larger river.

1. Introduction

As major land-ocean ecosystem connectors, inland waters are key sites for transport, transformation, and burial of carbon and nutrients (Kattner et al., 1999; Zhou et al., 2021). Dissolved organic matter (DOM) comprises the largest pool of active and exchangeable organic carbon on Earth, and plays a profound role in carbon cycling (Hansell and Carlson, 2014). Most organic carbon in aquatic environments is in the dissolved form, and the global dissolved organic carbon (DOC) flux from worldwide rivers into the ocean is estimated at approximately 0.25 Pg C yr^{-1} (Hedges et al., 1997; Raymond and Spencer, 2015). Riverine DOC fluxes are usually higher in large rivers with larger discharge. Greenhouse gas

---

* Corresponding author at: School of Geography, Nanjing Normal University, No.1 Wenyuan Road, Nanjing, 210023, China.
E-mail address: huangchangchun@njnu.edu.cn (C. Huang).

https://doi.org/10.1016/j.watres.2023.119812
Received 21 January 2023; Received in revised form 23 February 2023; Accepted 24 February 2023

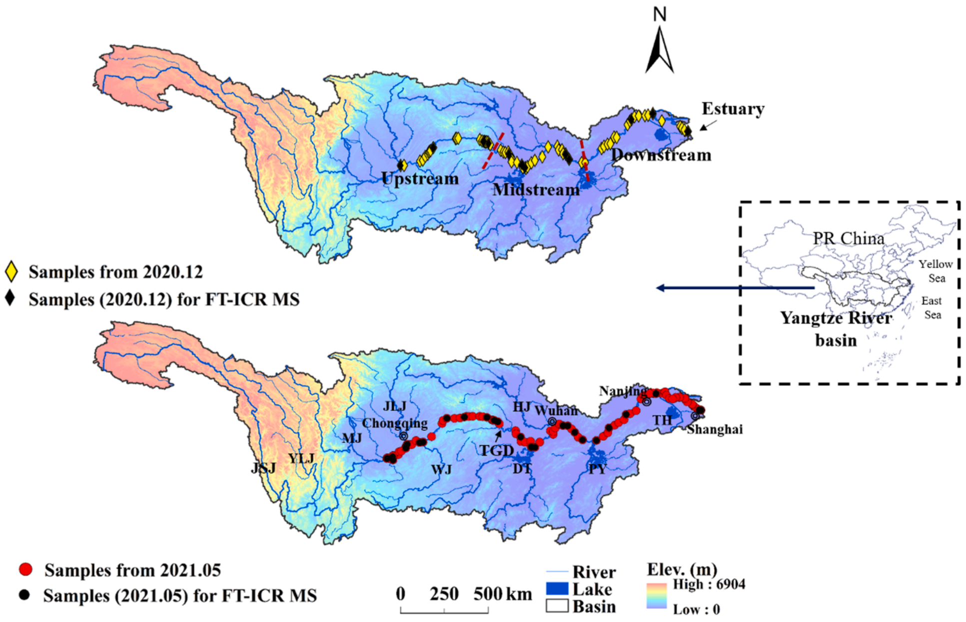

Fig. 1. Map of study area and sampling sites. Major tributaries and lakes are Jinshajiang River (JSJ), Yalongjiang River (YLJ), Minjiang River (MJ), Jialingjiang River (JLJ), Wujiang River (WJ), Hanjiang River (HJ), Dongting Lake (DT), Poyang Lake (PY) and Taihu Lake (TH). The Three Gorges Dam (TGD), as the worldwide largest hydroelectric dam, is located in the middle stream of Yangtze River and has been fully operated since 2006.

emissions, biological activity, and ecological stability of fluvial systems are closely related to the elemental, optical and molecular characteristics of DOM (Medeiros et al., 2015; Remington et al., 2011). Therefore, the spatial and temporal variability of the quantity and quality of DOM in large rivers has become a research hotspot in recent years (Bianchi et al., 2004; Spencer et al., 2009; Zhao et al., 2021a).

Riverine DOM is derived from multiple sources, including allochthonous DOM from soil and plant litters along tributaries and main river channels, autochthonous DOM from in situ primary production, and anthropogenic DOM from agricultural runoff, urban wastewater and fossil fuel combustion (Begum et al., 2022; Cleveland et al., 2004; Gonsior et al., 2011; Spencer et al., 2019; Zhang et al., 2021). The construction of dams and land use changes may also indirectly regulate source distributions for riverine DOM (Du et al., 2021; Kraus et al., 2011). For instance, agriculture can stimulate phytoplankton biomass growth and reduce dissolved oxygen concentration by increasing nutrient loadings, which leads to a higher proportion of autochthonous DOM in receiving waters (Chen et al., 2021).

Due to inherent absorbance and fluorescence properties, ultraviolet-visible spectroscopy (UV–Vis) and excitation-emission matrix fluorescence spectroscopy (EEM) combined with parallel factor analysis (PARAFAC) have been widely used to track DOM sources and components (Helms et al., 2008; Li et al., 2020; Osburn et al., 2016). However, traditional optical techniques have unavoidable limitations to explain the behavior of non-chromophoric and specific compounds within the DOM pool. In recent years, Fourier-transform ion cyclotron resonance mass spectrometry (FT-ICR MS) has been revealed as a powerful tool for identifying DOM compositions at the molecular level by detecting and assigning unique molecular formulae to thousands of mass spectra peaks (Behnke et al., 2021; Kellerman et al., 2015; Spencer et al., 2014). FT-ICR MS is also useful to trace photo/bio-degradation and other chemical reactions (e.g., methylation, sulfurization, hydrogenation and oxidation) during DOM cycling processes (Berg et al., 2019; Miranda et al., 2020; Schmitt-Kopplin et al., 2010). Furthermore, changes in stable carbon isotopic ratios ($\delta^{13}C$) are induced by photosynthesis, diagenetic and metabolic fractionation, thus $\delta^{13}C$ is a useful tool for tracking sources and biogeochemical transformation of organic carbon (Andrews et al., 1998; Nkoue Ndondo et al., 2021; Wu et al., 2007). $\delta^{13}C$ values for terrestrial C3 plant (−30‰ to −20‰) are significantly lower than for plankton in eutrophic lakes and seawater (−22‰ to −19‰), but are more positive than for plankton in freshwater (−32‰ to −26‰) (Derrien et al., 2018; Lamb et al., 2006; Zhao et al., 2021b). Additionally, the development of the MixSIAR model in R software based on a Bayesian framework allows quantification of the contribution of these diverse sources of organic matter in inland aquatic ecosystems (Meng et al., 2021; Stock et al., 2018).

The Yangtze River (China) is the largest river in Asia, and links mainland China with the East China Sea, the largest marginal sea in the north-western Pacific. Previous studies estimated DOC transport and air-water CO_2 fluxes in the Yangtze River, and found they were mainly controlled by temperature, river discharge, and precipitation (Liu et al., 2015; Zhai et al., 2007). Recently, the removal of riverine DOC via photo and microbial degradation and flocculation mechanisms has also been reported (Figueroa et al., 2021; Waiser and Robarts, 2004). However, it remains unclear how the DOM characteristics at elemental, optical and molecular levels change across the land-ocean continuum of this large river. Expected modifications in the ratios of allochthonous v. autochthonous sources and stable vs labile compounds commonly caused different dynamics of riverine DOM (Roth et al., 2019; Spencer et al., 2019). Moreover, previous studies were based on a limited number of sampling sites near the existing hydrological stations or short reaches of the Yangtze River (Bai et al., 2015; Wang et al., 2021). Due to various landform types and intense local human activities in the Yangtze River Basin, the amount and quality of DOM have been possibly altered dramatically over time. Therefore, it is necessary to conduct more precise investigations along the entire stream with higher spatial and temporal resolution.

In this study, surface water samples were collected from upstream to estuary of the Yangtze River (total distance: > 2300 km) during two contrasting seasons. Due to chemical complexity and diversity of DOM in a large river, we combined a set of analytical methods, including hydrological measurements, elemental, optical (absorbance and fluorescence), carbon isotope and molecular (FT-ICR MS) techniques. Our objectives were to: (1) investigate the abundance, sources and compositions of DOM at highly spatial resolution in two seasons; (2) clarify the transport and transformation of riverine DOM at spatial and temporal scales; and (3) explore the impacts of natural and anthropogenic forces on DOM cycle.

2. Materials and methods

2.1. Study site, sample collection and in situ data

The Yangtze River has a total length of 6300 km and a drainage basin area of 1808,500 km^2 from the Qinghai-Tibetan Plateau to the East China Sea (Fig. 1). Based on hydrologic and geographical characteristics, we divided the Yangtze River into three reaches: upstream reach (above Yichang city), midstream reach (from Yichang city to Hukou city) and downstream reach (from Hukou city to estuary). The Yangtze River Basin is characterized by a subtropical monsoon climate with a mean precipitation of 1054 mm (average years 1961–2019) (Zhou et al., 2021). Due to Asian ocean monsoons and anticyclone anomalies, $>$ 70% of annual rainwater, relatively higher temperature and UV-radiation occur between May and October. The Yangtze River Basin includes several large tributaries and lakes (indicated on Fig. 1), and is mainly covered by forest (38.6%), arable (29.5%), grassland (24.5%), residential (1.4%) and bare lands (2.81%) (Gao et al., 2010). Total population living in the Yangtze River Basin represents about one-third of China's population ($>$ 400 million), and economic productivity in the Yangtze River Basin is almost half of the Gross National Product of China. Detailed climatic and economic information is provided in Fig. S1.

This study was conducted along the main stream of the Yangtze River from upstream near Chongqing city to the estuary (Fig. 1). Surface water samples were collected with a 10 L Niskin bottle (pre-cleaned by pH=2 HCl-acidified water and ultrapure water) in December 2020 (samples YZD1 to 71) and in May 2021 (samples YZM1 to 114) from a research vessel. The two sampling periods had significant differences in monthly rainfall, air temperature and river discharge (Wang and Wu, 2021), the first representing the dry season and the second representing the early wet season. Each sample was divided into two aliquots. The first aliquot was immediately filtered through pre-combusted (450 °C for 6 h) GF/F filters (Whatman, 47 mm diameter). The filtrates and second aliquot samples were stored at 4 °C in the dark before analysis.

Basic water quality parameters, including water temperature (WT), specific conductivity (SpC), dissolved oxygen (DO), pH and water turbidity, were determined using a portable multi-parameter water quality probe (YSI ProDSS, U.S.A) and a palintest CT12 turbidimeter (Burlingda, British) at each sampling site (Fig. S2).

2.2. Geochemical, spectroscopic analysis and PARAFAC model

DOC concentration was measured using a total organic carbon analyzer (Shimadzu TOC-L, Japan) by the non-purgeable organic carbon (NPOC) assay method. Total nitrogen (TN), nitrate (NO_3^--N), ammonia (NH_4^+-N), and total phosphorus (TP) were measured by spectrophotometric methods based on (GB/T11893, 1989; HJ536, 2009; HJ636, 2012). These results are displayed in Fig. S3–4.

The UV–vis absorption spectra of DOM samples was scanned from 200 to 800 nm with 1 nm interval in a UV-3600 spectrophotometer (Shimadzu, Japan); the path length of the quartz cuvette was 1 cm, and ultrapure water was used as blank. The EEM data of DOM samples were measured with a FS5 spectrofluorometer (Edinburgh Instruments) using ultrapure water as a blank. The excitation (Ex) and emission (Em) scans were 200–450 nm (interval: 5 nm) and 250–600 nm (interval: 1 nm), respectively. Details on correction procedures for EEM results are shown in Supporting Information 1.1, and all fluorescence intensities were finally normalized to Raman units (R.U.) (Murphy et al., 2010). Details on the calculation and interpretation of commonly used spectral parameters, including absorption coefficients (a_λ), carbon-specific absorption at 254 nm ($SUVA_{254}$), spectral slope at the wavelength range of 275 to 295 nm ($S_{275–295}$), fluorescence index (FI), biological index (BIX) and humification index (HIX), can be found in Table S1.

PARAFAC modeling for all valid and corrected EEM data was conducted using MATLAB R2014b with the DOMFluor toolbox (Stedmon and Bro, 2008). Based on the residual and split-half analysis and comparison with the OpenFlour database (Murphy et al., 2014), five fluorescence components were identified, including three humic-like components (C1-C3) and two protein-like components (C4-C5) (Fig. S5 and Table S2). The relative abundance of each component was calculated by dividing the fluorescent intensity (F_{max}) of each component by total the fluorescent intensity (F_{max} of Ct).

2.3. Stable carbon isotopic analysis

The wet-oxidation method combining persulfate and heat has been previously employed for measuring the δ^{13}C of DOC ($\delta^{13}C_{DOC}$) (Lang et al., 2012; Zhou et al., 2015). The isotopic carbon composition of the CO_2 resulting from organic matter oxidation was determined with a MAT-253 isotope ratio mass spectrometer (Thermo Fisher Scientific, Bremen, Germany) coupled with a GasBench on-line high-precision gas headspace sampler (Thermo Fisher Scientific). Details can be found in the Supporting Information 1.2. We selected USGS 40 (L-glutamic acid, NIST) whose true δ^{13}C value is $-26.39 \pm 0.09‰$ as organic carbon standard. Each sample and standard were measured five times and the standard deviation of $\delta^{13}C_{DOC}$ was less than 0.4‰. Finally, all measurements were calibrated based on modified single-point anchoring normalization to remove the influence of the isotopic composition of the blank (Paul et al., 2007).

2.4. Pre-treatment, measurement and data analysis of FT-ICR MS

A total of 37 DOM samples (11 samples from the dry season and 26 samples from the wet season) were prepared for FT-ICR MS analysis by solid-phase extraction (SPE) with Bond Elut PPL cartridges (6 mL, 500 mg, Agilent) as previously described (Dittmar et al., 2008). Details can be found in the Supporting Information 1.3. Molecular analysis of extracted DOM was performed on a 21-tesla FT-ICR MS with negative electrospray ionization located at the National High Magnetic Field Laboratory in Tallahassee, Florida, USA (Smith et al., 2018). The broadband mass spectrum was collected from 100 averaged time-domain transients. Molecular formulae were assigned from mass spectral peaks with signals $>$ 6σ baseline root-mean-square noise (Behnke et al., 2021; Spencer et al., 2019) using the PetroOrg software (Corilo, 2015). Elemental combinations of $C_{1–45}H_{1–92}N_{0–4}O_{1–25}S_{0–2}$ and mass error $\leq$ 300 ppb were set to formulae assignments (Kellerman et al., 2018). These formulae with ^{13}C peaks, O/C $>$1 and H/C $>$ 2.5 were also removed. The modified aromaticity index (AI_{mod}), double-bond equivalent (DBE) and nominal oxidation state of carbon (NOSC) were calculated based on molecular formula (Kellerman et al., 2015; Koch and Dittmar, 2006; Stubbins et al., 2010). Molecular compounds were classified into: condensed aromatics (CA, $AI_{mod} > 0.66$), polyphenolics ($0.5 < AI_{mod} \leq 0.66$), highly unsaturated and phenolics, low O/C (HUPs, low O/C, $AI_{mod} \leq 0.5$, H/C $<$ 1.5, O/C $<$ 0.5), highly unsaturated and phenolics, high O/C (HUPs, high O/C, $AI_{mod} \leq 0.5$, H/C $<$ 1.5, $0.5 \leq$ O/C ≤ 0.9), aliphatic ($1.5 \leq$ H/C ≤ 2.0, O/C ≤ 0.9 and $N = 0$), peptide-like ($1.5 \leq$ H/C ≤ 2.0, and $N > 0$) and sugar-like (O/C > 0.9). The semi-quantitative contributions of the compounds (e.g., aliphatic) and elemental molecules (e.g., CHO) were calculated by the sum of the relative abundances of each compound or elemental molecules divided by the summed relative abundances of all assigned formulae in each sample (Behnke et al., 2021), which were expressed as relative abundance percentages (e.g., aliphatic%RA, CHO%RA). All FT-ICR MS data files and elemental composition assignments are publicly-available via the Open Science Framework DOI: 10.17605/OSF.IO/DWBKT (https://osf.io/dwbkt/).

2.5. Other statistical analyses

Once the normality of variables was checked, one-way analysis of variance (one-way ANOVA) and Kruskal-Wallis test were performed to assess the significance of DOM differences among seasons and river

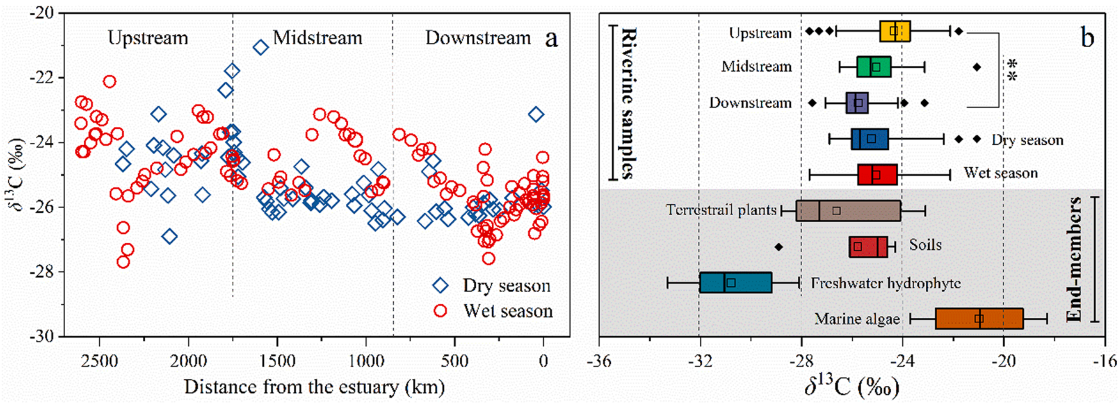

Fig. 2. $\delta^{13}C$ values of DOC samples along the Yangtze River (a), and comparisons between $\delta^{13}C$ values of samples and end-members collected from the related references, including terrestrial plants, soils, freshwater hydrophyte and marine algae (b). The boxes represent 25%–75% quartile, whiskers represent 1.5·IQR, black circles squares represent mean values, and black diamonds represent outliers.

reaches in SPSS 19.0 software. Significance was reported as $^{*}p < 0.05$, $^{**}p < 0.01$, $^{***}p < 0.001$. Spearman correlation analysis was conducted in R 4.2.0 with the “Hmisc” package. Principal component analysis (PCA) was used to further examine DOM variability in R 4.2.0 with the “factoextra” package, and all variables were scaled to unit variance before PCA.

3. Results and discussion

3.1. Concentrations, fluxes and sources of DOC in the Yangtze River

The DOC concentration along the Yangtze River ranged from 1.30 mg C L^{-1} to 3.20 mg C L^{-1} (Average ± Standard Deviation: 1.83 ± 0.40 mg C L^{-1}) in the dry season and 1.15 mg C L^{-1} to 3.43 mg C L^{-1} (1.68 ± 0.26 mg C L^{-1}) in the wet season (Fig. S3a-b). The DOC concentration was not significantly different between the two seasons, implying that the impoundment of the Three Gorges Dam during the dry season did

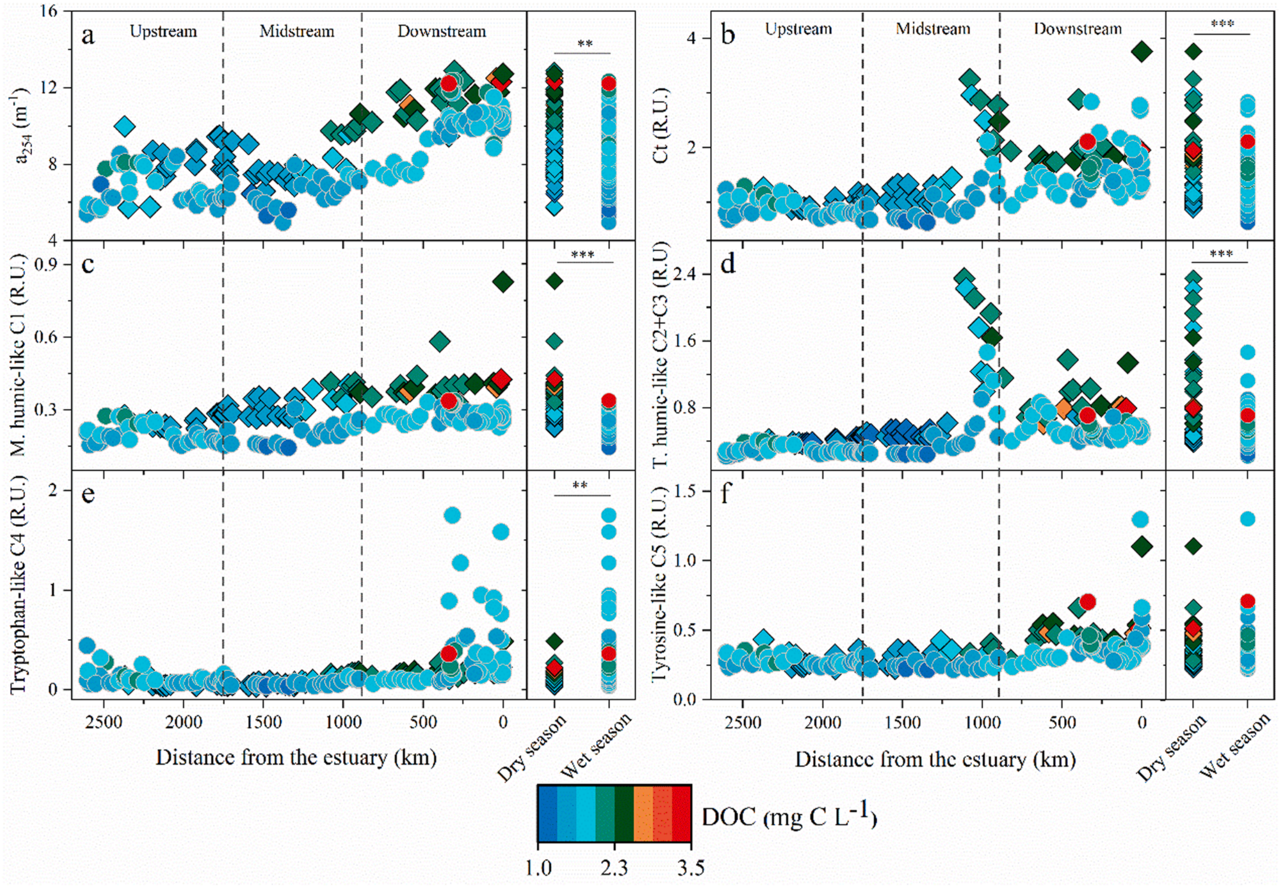

Fig. 3. a_{254} (a), F_{max} of Ct (b), microbial (M.) humic-like (c), terrestrial (T.) humic-like (d), tryptophan-like (e) and tyrosine-like component (f) along the Yangtze River. The rhombuses and circles presented samples collected during dry season and wet season, respectively. The color of the rhombuses and circles is proportional to the DOC concentration.

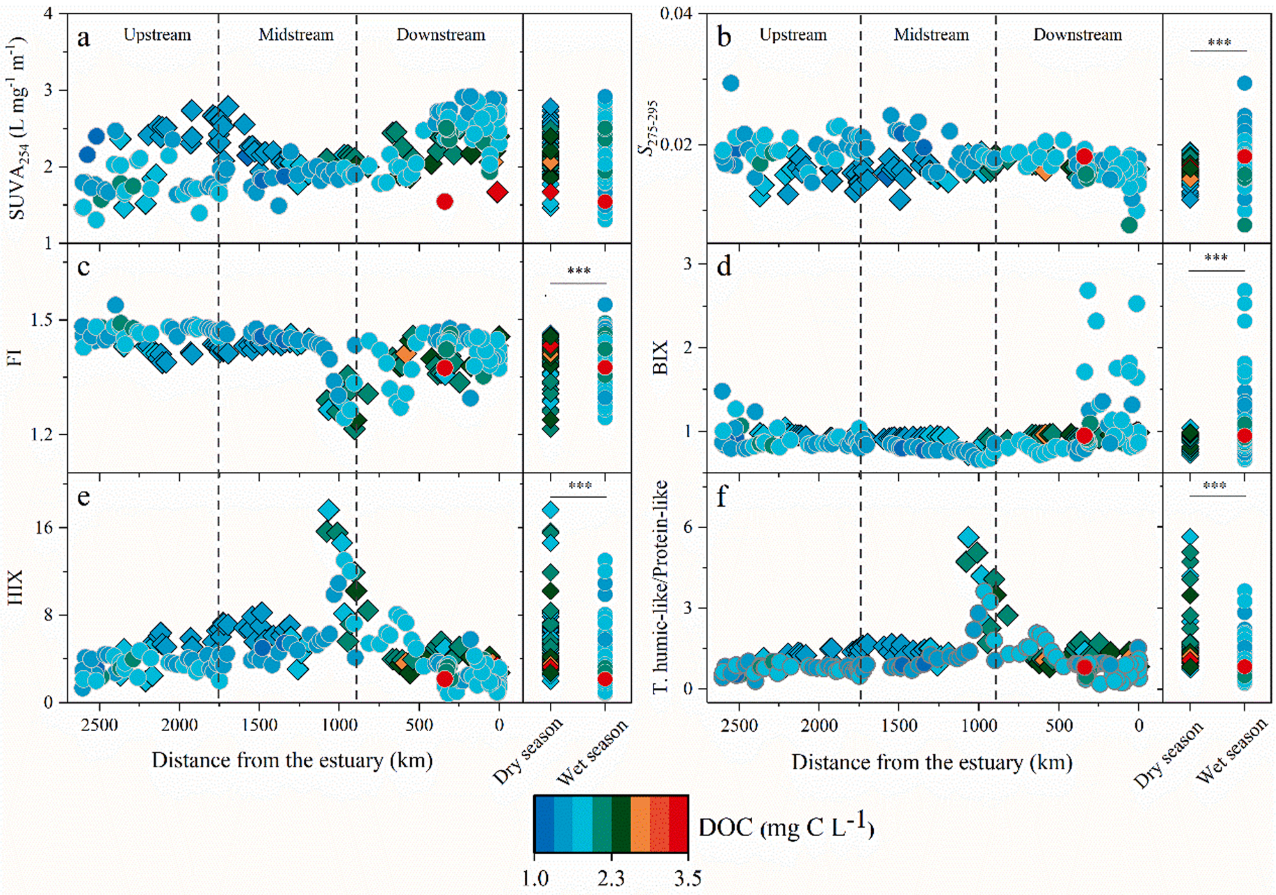

Fig. 4. SUVA$_{254}$ (a), $S_{275–295}$ (b), FI (c), BIX (d), HIX (e) and the ratio of T. humic-like to protein-like component (f) along the Yangtze River. The rhombuses and circles presented samples collected during dry season and wet season, respectively. The color of the rhombuses and circles is proportional to the DOC concentration.

not lead to more DOC decomposition though it could increase time residence of river water. According to daily field records at hydrometric stations, the DOC flux was estimated to be approximately 0.038–0.094 Tg C for the dry season month and 0.063–0.19 Tg C for the early wet season month, respectively. Higher DOC flux during the wet season supports previous studies showing that discharge could control DOC dynamics in lakes or rivers (Bao et al., 2015; Liu et al., 2015). The DOC flux in this study is much lower than other large rivers, such as the Mississippi, Amazon and Congo rivers, which is attributed to comparatively low DOC concentration in the Yangtze River (Liu et al., 2015). The average DOC value was highest downstream (1.94 ± 0.37 mg C L^{-1}), followed by upstream (1.60 ± 0.19 mg C L^{-1}) and midstream (1.60 ± 0.23 mg C L^{-1}, Fig. S6a). The significant increase of DOC from upstream reach to estuary reflected carbon accumulation with water flow. Although the dense population and rapid urbanization downstream likely increased DOC inputs to the river (Fig. S1a-b), the added DOC was relatively low (< 4 mg C L^{-1}) due to “green development” performed in China since 2016 (Zhou et al., 2021). Moreover, the significantly positive relationship between DOC concentration and water turbidity indicated that particulate organic carbon (POC) could be a source of DOC, which makes river browner, impacting light penetration depth into water ($p < 0.001$, Fig. S3d).

$\delta^{13}C_{DOC}$ varied between −26.90‰ and −21.06‰ with an average value of −25.24 ± 1.13‰ in the dry season, and between −27.69‰ and −22.12‰ with an average of −25.05 ± 1.16‰ in the wet season (Fig. 2a). There was no significant difference in $\delta^{13}C_{DOC}$ values between the two seasons ($p > 0.05$). $\delta^{13}C_{DOC}$ slightly increased with distance from the estuary, which was higher upstream (−24.34 ± 1.20‰) than midstream (−25.04 ± 1.01‰) and downstream (−25.76 ± 0.79‰). Based on the $\delta^{13}C_{DOC}$ values, the samples from different seasons and river reaches might have the same sources, and/or the intense mixing of river water made the $\delta^{13}C_{DOC}$ signature to be more homogeneous along the Yangtze River. Here, we found that riverine DOC was mainly originated from allochthonous and autochthonous organics. The $\delta^{13}C$ distribution of allochthonous organics included terrestrial soil and plants litters around the watershed (range: −28.9~−23.1‰, average: −26.2 ± 1.9‰, Fig. 2b) are close to our samples’ $\delta^{13}C_{DOC}$ values (Sun et al., 2021; Wu et al., 2007), but the $\delta^{13}C$ values of autochthonous sources were more negative (range: −33.3~−28.1‰, average: −30.8 ± 1.7‰, Fig. 2b) because hydrophyte preferentially utilized dissolved ^{12}C-rich CO_2 ($\delta^{13}C$: ~7‰) during photosynthesis (Marty and Planas, 2008). Since marine algae preferred bicarbonate ($\delta^{13}C$: ~0‰) as carbon sources instead of dissolved CO_2, their $\delta^{13}C$ increased to a relatively high average value (−20.9 ± 1.9‰) (Lamb et al., 2006). The higher $\delta^{13}C$ value of autochthonous sources was also found in some eutrophic inland lakes (e.g., Taihu lake and Dianchi lake) because dissolved CO_2 was depleted to near-zero value (Li et al., 2022; Meng et al., 2021), but the phenonmenon was rare in the Yangtze River. Therefore, we suggested that allochthonous organic matter played a prominent contribution for the riverine DOM pool, which is consistent with some previous study results (Wen et al., 2021; Wu et al., 2007). Conversely, autochthonous carbon sources did not contribute significantly. Due to high flow, turbidity, water depth, and rocky bottom, in situ phytoplankton and submerged plants growth in the Yangtze River is limited (Wang et al., 2014). Some overlaps among the $\delta^{13}C$ ranges of allochthonous and autochthonous end-members likely affect the accuracy of estimated results by Bayesian mixing model. Therefore, we should combine other techniques to provide more evidence for the diverse origins of riverine DOM, as will be discussed in next sections.

3.2. Variations in optical properties of riverine DOM

Optical properties of DOM showed obvious spatial difference along the Yangtze River (Fig. 3-4 and Fig. S6). a_{254} gradually increased downstream, varying between 4.94 m^{-1} and 12.90 m^{-1} (Fig. 3a). $SUVA_{254}$ had a significantly higher value downstream (2.38 ± 0.33 L mg^{-1} m^{-1}) than midstream (2.04 ± 0.24 L mg^{-1} m^{-1}) and upstream (1.96 ± 0.38 L mg^{-1} m^{-1}, $p < 0.001$, Fig. S6c). The average $S_{275–295}$ value was closed among downstream (0.016 ± 0.002), midstream (0.016 ± 0.003) and upstream (0.016 ± 0.003, Fig. 4b), and the difference didn't show statistical significance ($p > 0.05$, Fig. S6d). These suggested that chromophoric DOM (CDOM) was constantly resupplied by surface runoff between midstream and downstream reaches. The highest abundance of terrestrial (T.) humic-like components (C2 and C3, range: 0.22–2.35 R.U.) and the low FI value (range: 1.22–1.76) indicated that the Yangtze River was mainly associated with imported terrestrial humus leached from soils and litters. From the notably higher F_{max} value of T. humic-like components midstream (0.68 ± 0.53 R.U., $p < 0.05$, Fig. S6g), we inferred that the additional terrestrial fluorescent DOM (FDOM) was transported by the Han River which is the longest tributary of the Yangtze River. Meanwhile, HIX was obviously higher midstream (6.99 ± 3.30) than upstream (3.82 ± 1.17) and downstream (3.47 ± 1.58, $p < 0.001$, Fig. S6l), but FI decreased midstream (1.40 ± 0.07, Fig. 4c). Increased amounts of T. humic-like components elevated the humification degree and terrestrial signal of DOM. The F_{max} of the microbial (M.) humic-like component (C1) and two protein-like components (C4 and C5) gradually increased downstream (Fig. 3c and e-f), reflecting enhanced microbial metabolism and primary production which were closely related to densely agricultural and urban activities downstream (Chen et al., 2021; Tang et al., 2020). The significantly higher BIX downstream (1.06 ± 0.39, $p < 0.01$, Fig. S6k) also pointed to a greater contribution of freshly autochthonous inputs. However, the autochthonous production was still lower throughout the whole river based on average BIX < 1 and a ratio of T. humic-like component to protein-like component > 1. Consequently, terrestrial organic matter possibly became the dominant organic carbon source to for the aquatic food web. The C3/C4 grasses and invertebrates-derived nutrients on land could be continuously assimilated by primary consumers, contributing to consumers at higher trophic levels (Allan et al., 2003; Leite et al., 2002).

Furthermore, the characteristics of both CDOM and FDOM significantly changed from dry to wet seasons (Fig. 3-4). a_{254} and F_{max} of Ct, M. humic-like C1 and T. humic-like components (C2 and C3) significantly increased by 0.97 m^{-1}, 0.11 R.U. and 0.30 R.U. on average in the dry season compared with those in the wet season ($p < 0.01$). Despite terrestrial inputs would increase into Yangtze River via high runoff during wet season (Pang et al., 2021), increased river discharge eventually diluted CDOM and humic-like FDOM concentrations (Fig. S1c). On the other hand, enhanced solar UV radiation in summer promoted the penetration of light in water and rapidly decomposed photo-reactive substances, for example, CDOM and terrestrial humic-like FDOM. In contrast, the F_{max} of tryptophan-like C4 and BIX had significantly higher values in the wet season ($p < 0.01$). Phytoplankton growth and intense microbial activities would promote in situ primary production under warm temperature in the wet season (Fig. S1d), which released freshly protein-like fractions. $S_{275–295}$ and FI significantly decreased by 0.002 and 0.04 on average from wet season to dry season ($p < 0.001$), and HIX significantly increased by 1.84 on average from wet season to dry season ($p < 0.001$). The seasonal cycle and hydrologic change left relatively more CDOM and humic-like FDOM, and meanwhile reduced protein-like FDOM in the dry season, which increased the humification degree and terrestrial signal of riverine DOM. Overall, the total content of optical substance tended to accumulate downstream or in dry season, but natural and anthropogenic factors directly or indirectly impacted the complexity of optical structures and components.

3.3. General molecular signatures by FT-ICR MS

The number of molecular formulae detected via FT-ICR MS analysis was in the range of 11,468 to 16,750 depending on the 37 samples. The total number of formulae was 27,590, and the formulae pool would be gradually more saturated with increasing samples, suggesting these riverine samples were highly representative. The number of molecular formulae in the Yangtze River is higher than in Greenland glacier streams and a Pacific temperate lake, and similar to the Mississippi River (Johnston et al., 2022; Kellerman et al., 2021; Vaughn et al., 2021). Larger rivers crossing complex watersheds generally show a higher number of DOM formulae. The majority of molecular mass covered the range of 200–1000 Da (Fig. S7a), and showed a normal distribution centered at 630.30 Da (median value). A total of 6895 common formulae was ubiquitous among all samples, and usually appeared in the core of the van Krevelen (V-K) plot (O/C: 0.50 ± 0.12, H/C: 1.14 ± 0.22, Fig. S7b).

The calculation of the relative abundance of elemental compositions (Fig. S8) indicated that CHO molecules (64.14 ± 2.74%RA) dominated, followed by CHON (24.18 ± 2.21%RA), CHOS (10.69 ± 2.29%RA) and CHONS molecules (0.99 ± 0.34%RA). Based on O/C, H/C and AI_{mod}, molecular formulae were further divided into relatively stable compound groups (i.e., CA, polyphenolics and HUPs) and active compound groups (i.e., sugar-like, peptide-like and aliphatic, Fig. S7b). HUPs compound had the highest relative abundance (44.18 ± 2.16%RA at low O/C, 43.49 ± 2.52%RA at high O/C), followed by aliphatic (5.39 ± 1.54%RA) and polyphenolics compound (5.00 ± 0.79%RA) (Fig. S8). The other compounds represented less than 1%RA. HUPs compounds were mainly derived from lignin metabolism, and polyphenolics compounds were derived from terrestrial vascular-plants, but aliphatic compounds were usually produced by the fatty acids of phytoplankton (Behnke et al., 2021). These further supported our isotopic and optical results on the overwhelming contribution of allochthonous DOM throughout the Yangtze River. Medeiros et al. (2016) identified a set of 184 specific formulae (referred as "t-peaks") as plausibly indicative of the presence of terrigenous DOM based on FT-ICR MS data from four rivers from different regions around the world, including the Arctic (Kolyma River), subtropical (Altamaha River) and equatorial (Amazon and Congo Rivers) regions. These "t-peaks" were also found along the Yangtze River (n: 142–177), and 139 "t-peaks" were continuously observed from upstream to downstream reaches in both seasons (Table S3). Worldwide large rivers have been confirmed to be important pools of terrigenous carbon on Earth, and could export the part that escaped from photo/bio-degradation and flocculation to coastal region and even the deep ocean.

The different proportions of compounds with different elemental compositions could control the inherent structural characteristics (e.g., reactivity and persistence). To compare them, we calculated weight-averaged (wa) values of all FT-ICR MS parameters based on their initial values divided by the relative intensity of each peak (Table S4). The $mass_{wa}$ ranged from 518.55 to 567.10 Da with an average value of 540.95 ± 11.03 Da. AI_{mod-wa} ranged from 0.25 to 0.29, and the average value was almost 2.7-fold higher than that of algal extracts (AI_{mod}: 0.11, Lee et al., 2019). DBE_{wa} varied between 11.07 and 12.54 with an average value of 11.67 ± 0.42. These reflected that the abundant terrestrial materials (e.g., HUPs and polyphenolic compounds) raised the overall molecular weight, aromaticity and unsaturated degree of DOM in the Yangtze River. The average $NOSC_{wa}$ value of −0.12 ± 0.03 was more positive than that of protein-like substance (−0.7), but fit with the NOSC range of lignin-like substance (−0.2 to −0.1), indicating a reduced state of carbon (Zhou et al., 2019). O/C_{wa} and H/C_{wa} ranged from 0.47 to 0.51 and 1.14–1.22, and had an average value of 0.50 ± 0.01 and 1.18 ± 0.02, respectively. The relatively higher O/C ratio and lower H/C ratio indicated that our DOM samples were less active due to a lower contribution of freshly autochthonous organic matter (e.g., aliphatic and peptide-like compounds).

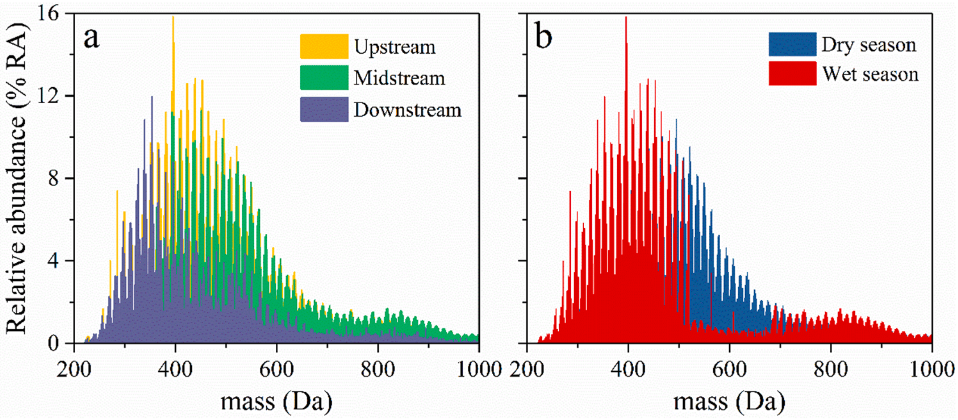

Fig. 5. FT-ICR MS with a mass range between 200 and 1000 Da of highlighted molecular formulae of three reaches (a) and two seasons (b) in the Yangtze River.

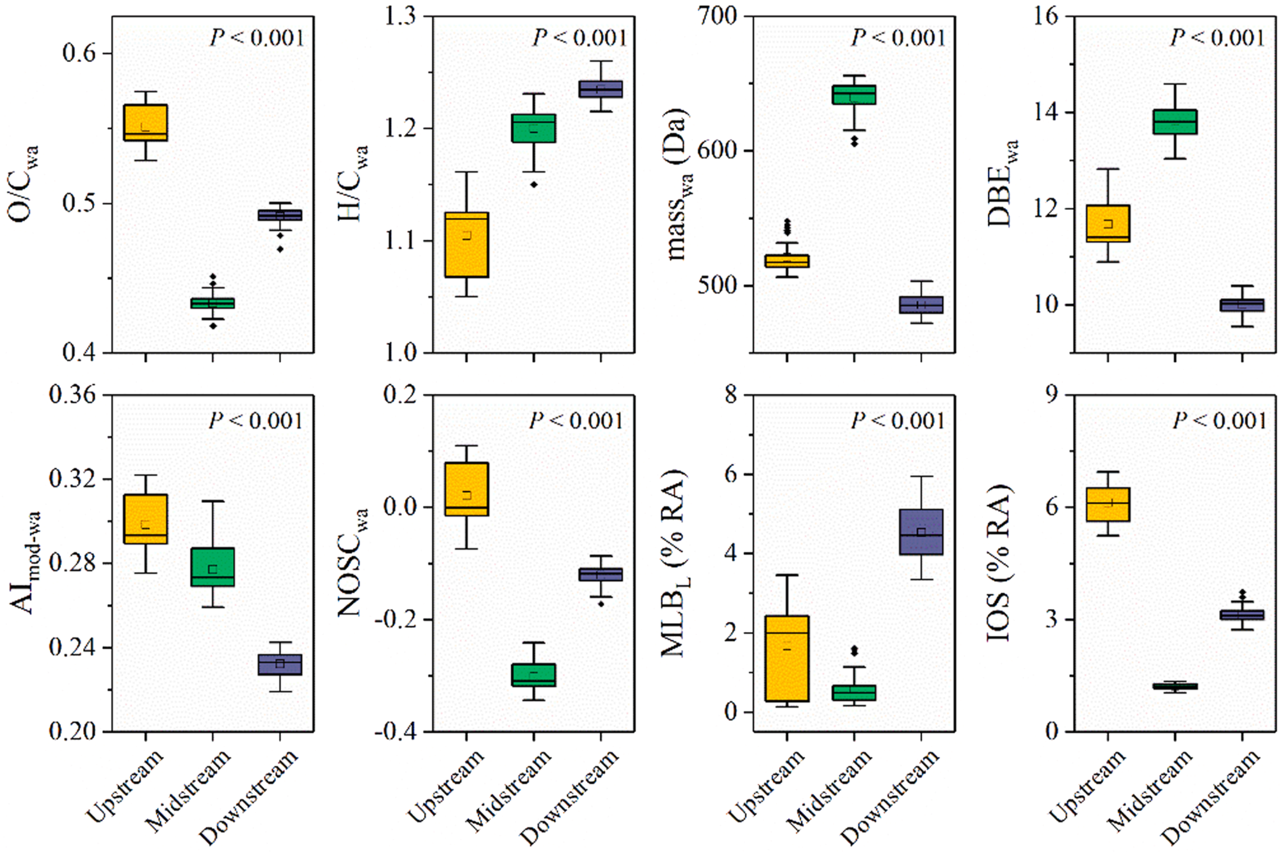

Fig. 6. Box plots showing the significant difference of O/C_{wa}, H/C_{wa}, $mass_{wa}$, DBE_{wa}, AI_{mod-wa}, $NOSC_{wa}$, MLB_L%RA and IOS%RA of highlighted molecular formulae of three reaches. The boxes represent 25%–75% quartile, whiskers represent 1.5·IQR, black circles squares represent mean values, and black diamonds represent outliers.

3.4. Highlighted formulae selected from different riverine reaches and seasons

The total number of molecular formulae assigned upstream (14 samples), midstream (15 samples) and downstream (8 samples) was 23,531, 24,866 and 22,686, respectively. To better understand pronounced variations of DOM molecules during the stream longitudinal process, we screened out the highlighted molecular formulae of three reaches by comparing their average relative abundance of all mass peaks. The results showed downstream samples had the highest number of highlighted formulae (n = 11,650), followed by midstream samples (n = 9190) and upstream samples (n = 6750). Due to abundant common formulae, these highlighted formulae of different reaches piled together in V-K plots (Fig. S9). However, the average mass of the highlighted formulae midstream (713.03 Da) was higher than that upstream (621.93 Da) and downstream (581.91 Da, Fig. 5a).

For molecule-compound fractions (Table S5), the highlighted formulae upstream was mostly consisted of CHO molecules (29.91%RA) and HUPs with high O/C compound (23.58%RA). CHOS and CHON molecules with HUPs with low O/C, polyphenolics and aliphatic compounds also had a significant contribution (> 1%RA). Molecular formulae were characterised as highly oxidized and aromatic. The

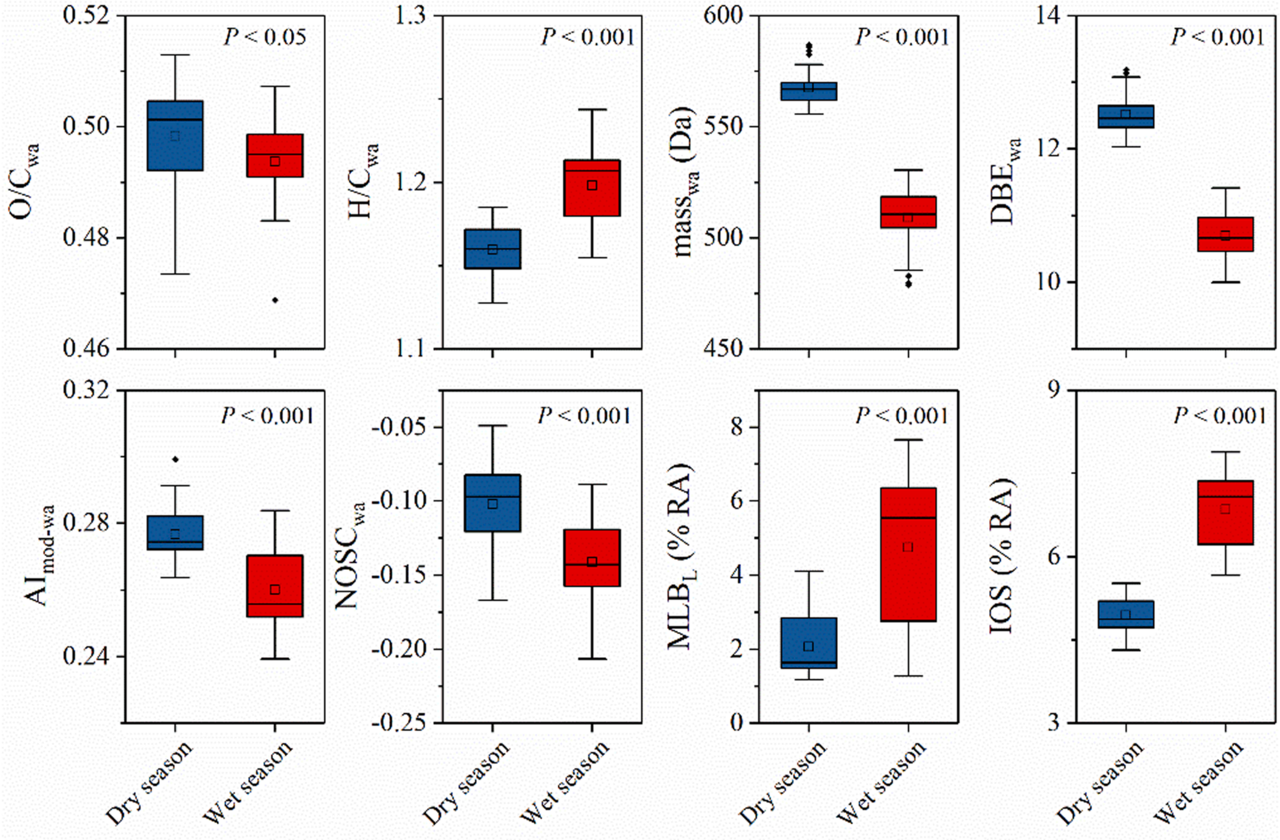

Fig. 7. Box plots showing the significant difference of O/C$_{wa}$, H/C$_{wa}$, mass$_{wa}$, DBE$_{wa}$, AI$_{mod-wa}$, NOSC$_{wa}$, MLB$_L$%RA and IOS%RA of highlighted molecular formulae of two seasons. The boxes represent 25%–75% quartile, whiskers represent 1.5·IQR, black circles squares represent mean values, and black diamonds represent outliers.

"island of stability" (IOS) occupying a narrow range of molecular formulae (O/C: 0.52 ± 0.10, H/C: 1.17 ± 0.13, mass: 360 ± 28 and 497 ± 51 Da) was considered to be the most stable fraction (Kellerman et al., 2018). IOS had a higher abundance among the highlighted formulae upstream and was positively correlated with HUPs with high O/C compound (Fig. 6 and S10), suggesting that they are recalcitrant compounds with abundant carboxylic-rich alicyclic molecules mainly originated upstream and could be long-distance transported by river and finally stored in East China Sea. In the midstream reach, the highlighted formulae were rich in CHO molecules (22.22%RA) and HUPs with low O/C compound (20.84%RA, Table S5), resulting in highly unsaturated, reduced and higher molecular weight DOM. Meanwhile, the relative abundance of CHON molecules increased to 4.61%RA, but the relative abundance of HUPs with high O/C and polyphenolic compounds decreased greatly. The consumption of oxygen-rich and aromatic molecules between upstream and midstream reaches might be caused by photodegradation, dilution and precipitation with iron minerals (Kamjunke et al., 2019). In the highlighted formulae downstream, the relative abundance of heteroatomic molecules markedly increased (CHON: 17.18%RA, CHOS: 6.71%RA) but CHO molecules decreased to 12.01% RA (Table S5). HUPs compound still had the highest abundance, but the added aliphatic compound (3.92%RA) reduced DOM unsaturation (higher H/C and lower DBE, Fig. 6). Moreover, molecules above the microbial lability boundary (MLB$_L$, $H/C \geq 1.5$, D'Andrilli et al., 2015) were abundant downstream, reflecting that the overall lability of molecules usually increased with more aliphatic and peptide-like compounds.

Regarding seasonality, the total number of molecular formulae assigned in the dry season (11 samples) and wet season (26 samples) was 19,751 and 24,074, respectively. We also compared average relative abundance of all mass peaks to find the highlighted molecular formulae which could better reflect seasonality. Samples in the dry season had less numbers of highlighted formulae ($n = 11{,}694$) than samples in the wet season ($n = 15{,}896$, Fig. S11). The mass distributions, major elemental compositions and molecular compositions of highlighted formulae were different among the two seasons (Fig. 5b and Table S6). The relative abundance of CHO and CHON molecules was higher in the dry season, and most of them were HUPs and polyphenolic compounds, but CHOS molecules had a higher relative abundance in the wet season, and most of them were HUPs and aliphatic compounds. These compositional changes from dry to wet seasons also influenced the structural characteristics of molecules. In the wet season, highlighted formulae showed a higher H/C ratio and lability by addition of aliphatic or MLB$_L$ compounds, but that in dry season had relatively higher oxidized, aromatic, unsaturated and molecular weight characteristics (Fig. 7). We also found that increased discharge during the wet season contributed more IOS in the Yangtze River (Fig. 7), which was consistent with previous report (Kurek et al., 2022). As a highly-degraded refractory product, IOS was likely independent of its initial properties and sources.

3.5. *Compositional assembly of riverine DOM as determined by PCA*

To explore the differences of DOM pool in diverse riverine reaches or seasons, we conducted five PCA using isotopic and optical data in conjunction with abundant molecules (%RA > 1) with highlighted formulae. PC2 loading (Fig. 8a) indicated the CHO molecules and HUPs with high O/C and polyphenolic compounds which had highest abundance in the highlighted formulae upstream were positively related to M. humic-like component% and $\delta^{13}C_{DOC}$, but were negatively correlated with a_{254}, SUVA$_{254}$, TP and TN. Additionally, there was a significantly

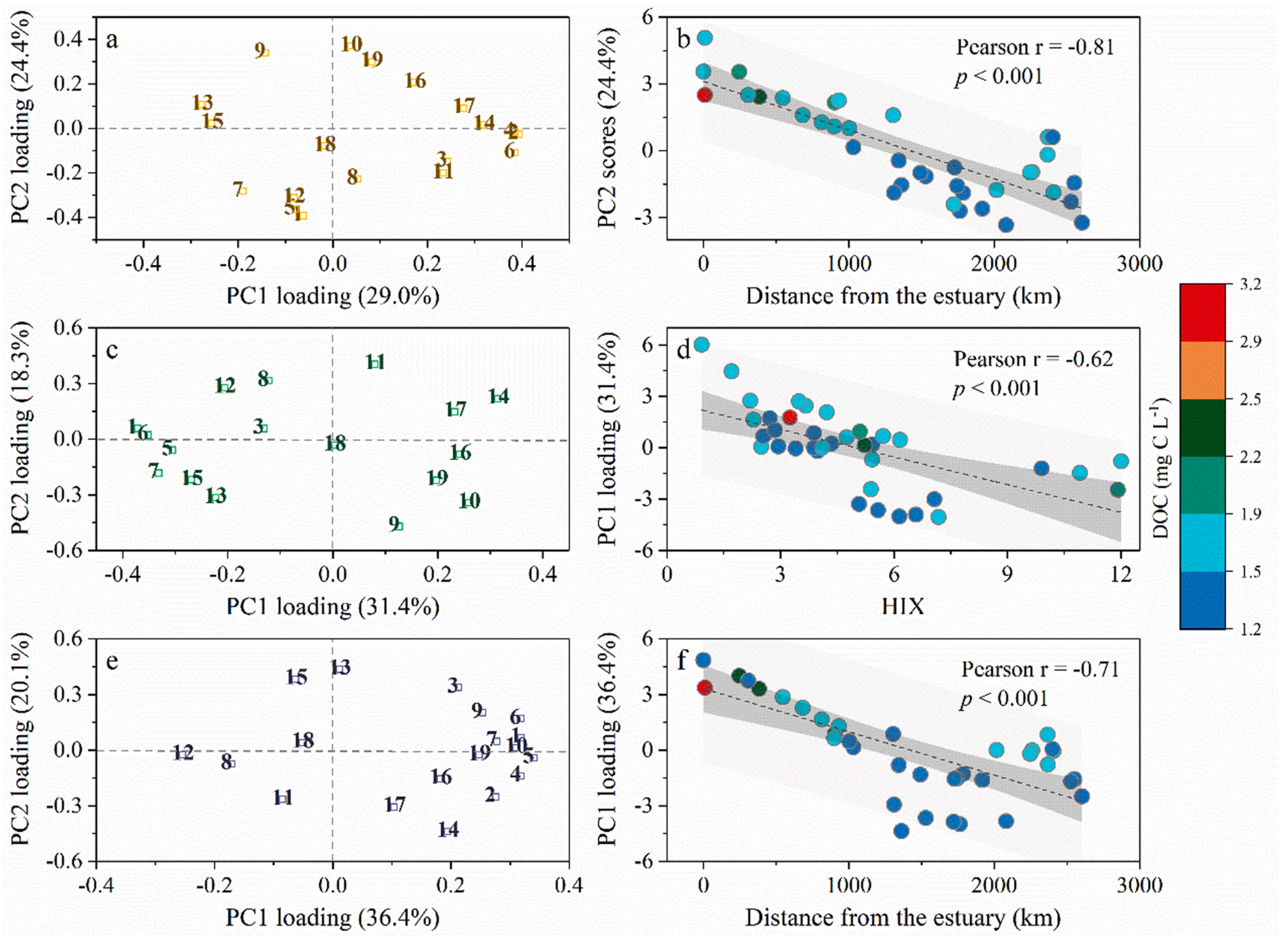

Fig. 8. PCA loadings of isotopic ratio, optical parameters and major FT-ICR MS molecules (%RA > 1) of highlighted formulae upstream (a), and relationship between PC2 scores and distance from the estuary (b). PCA loadings of isotopic ratio, optical parameters and major FT-ICR MS molecules (%RA > 1) of highlighted formulae midstream (c), and relationship between PC1 scores and HIX (d). PCA loadings of isotopic ratio, optical parameters and major FT-ICR MS molecules (%RA > 1) of highlighted formulae downstream (e), and relationship between PC1 scores and distance from the estuary (f). In PCA loading plots, 1: CHO%RA, 2: CHOS%RA, 3: CHON%RA, 4: Aliphatic%RA, 5: HUPs with high O/C%RA, 6: HUPs with low O/C%RA, 7: Polyphenolics%RA, 8: $\delta^{13}C_{DOC}$, 9: a_{254}, 10: $SUVA_{254}$, 11: $S_{275-295}$, 12: M. humic-like C1%, 13: T. humic-like C2 and C3%, 14: protein-like C4 and C5%, 15: HIX, 16: TN, 17: NO_3^--N, 18: NH_4^+-N, 19: TP.

negative relationship between PC2 scores and distance from the estuary ($p < 0.001$, Fig. 8b). We inferred that the DOM pool upstream had low CDOM content, but was enrich in highly oxygenated, aromatic and less hydrogenated molecules and microbial FDOM components. Comprehensive ecological restoration in the Yangtze River basin has increased the forest coverage upstream to approximately 50%. A previous study reported molecular assemblages in forest stream had high O/C ratio and aromatic fingerprints due to the dominance of HUPs and polyphenolic compounds from terrestrial surface soils and litter layers (Spencer et al., 2019). However, longitudinally higher flow along the river possibly limited the accumulation of terrestrial organic-rich materials, leading to lower CDOM content upstream. The dominant molecules (e.g., CHO% RA) and compounds (e.g., HUPs with low O/C%RA) midstream were strongly correlated with T. humic-like component% in PC1 negative loading (Fig. 8c), and PC1 scores had a significantly negative correlation with HIX value ($p < 0.001$, Fig. 8d). The inflow of the Han River contributed to greater amounts of terrestrial humic-rich fractions, coupled with low-oxidized and high molecular weight HUPs compounds. They were more concentrated midstream than in other two reaches and were considered as typical compositions of the DOM pool midstream. The major elemental composition and molecules of the highlighted formulae downstream with a_{254}, $SUVA_{254}$, protein-like component%, TP and TN appeared in the PC1 positive loading (Fig. 8e). PC1 scores also had a significantly negative correlation with the distance from the estuary ($p < 0.001$, Fig. 8f). As cropland and urban land increased, agricultural practices, anthropogenic sewage and associated enhanced primary productivity resulted in more heteroatomic formulae and labile aliphatic and protein-like compounds in the DOM pool downstream. One of the most widely used surfactants for detergents in China is linear alkylbenzene sulfonates (LAS), which are composed of O_3S- compounds and can be degraded into O_5S- compounds under aerobic condition (Gong et al., 2022; Gonsior et al., 2011). In this study, these O_3S and O_5S- compounds had a significantly positive correlation with CHOS molecules ($p < 0.001$, Fig. S12). On the other hand, reductive sulfurization reaction probably also increased the abundance of CHOS molecules by exchanging one O atom by one S atom (Gomez-Saez et al., 2016). Moreover, CDOM content gradually increased downstream due to slow river flow and additional autochthonous organics.

Major molecules and compounds of highlighted formulae in the dry season were strongly correlated with HIX and T. humic-like component % in PC1 negative loading (Fig. 9a-b). Major molecules and compounds of highlighted formulae in the wet season were closely correlated with protein-like component%, NO_3^--N, TN and TP in PC1 positive loading (Fig. 9c-d). During the cold/dry seasons, the relatively weaker solar radiation and water dilution left more aromatic, oxygenated, higher unsaturated and molecular weight compounds (e.g., HUPs and polyphenolics) and terrestrial humic-like components, and meanwhile the

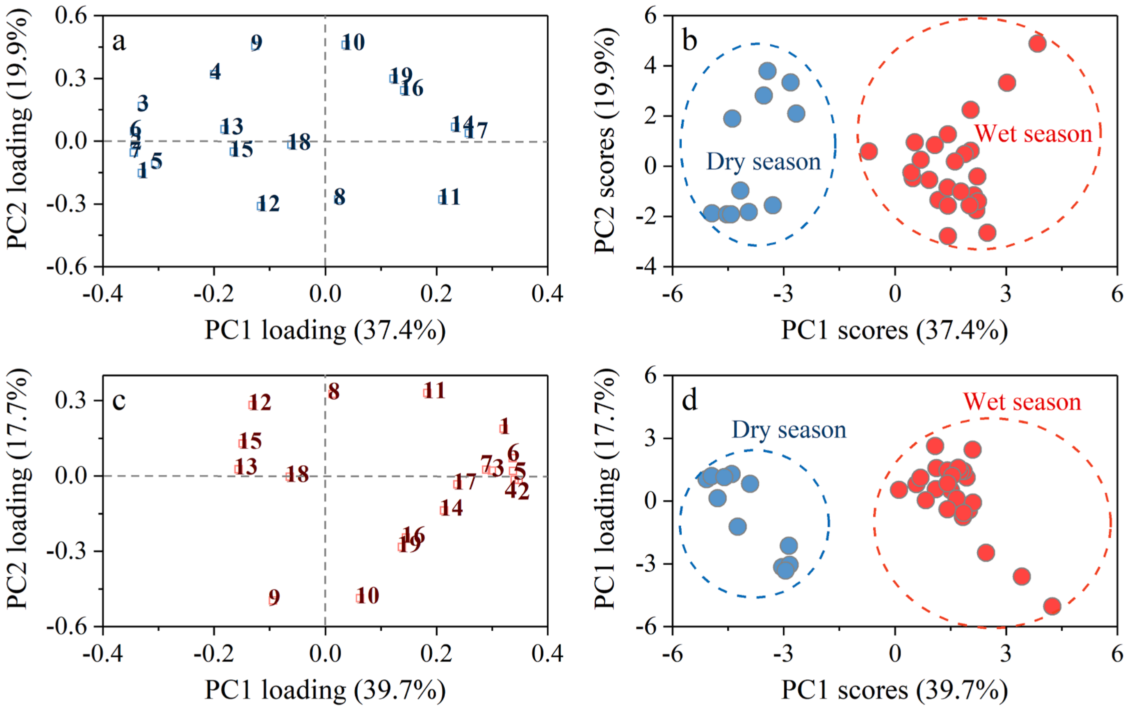

Fig. 9. PCA loadings and scores of isotopic ratio, optical parameters and major FT-ICR MS molecular compositions (%RA > 1) of highlighted formulae in dry season (a-b), and wet season (c-d). In PCA plots, 1: CHO%RA, 2: CHOS%RA, 3: CHON%RA, 4: Aliphatic%RA, 5: HUPs with high O/C%RA, 6: HUPs with low O/C%RA, 7: Polyphenolics%RA, 8: $\delta^{13}C_{DOC}$, 9: a_{254}, 10: $SUVA_{254}$, 11: $S_{275-295}$, 12: M. humic-like C1%, 13: T. humic-like C2 and C3%, 14: protein-like C4 and C5%, 15: HIX, 16: TN, 17: NO_3^--N, 18: NH_4^+-N, 19: TP.

autochthonous contribution was very low due to the absence of biological processes. A few aliphatic and peptide-like compounds derived from the microbial metabolism in soils were possibly transported to the river via surface runoff and groundwater, and could be preserved due to cold temperatures in winter (Behnke et al., 2021). During the warm and wet season, increased temperature and nutrients inputs from agricultural activities promoted phytoplankton growth and microbial activities that released some freshly autochthonous DOM fractions, such as aliphatic and protein-like compounds. These bio-available substances could serve as an additional substrate for primary production and microbial communities in the aquatic environment, while their degradation would produce some greenhouse gasses emission. Overall, our findings well demonstrated that rapid response of DOM pool in a large river to surrounding conditions, which play a greater influence on biogeochemical cycling of riverine and even coastal environments.

4. Conclusion

The $\delta^{13}C_{DOC}$ values indicated the dominance of allochthonous over autochthonous DOM, as confirmed by the high fluorescence intensity of the humic-like components identified by EEM-PARAFAC and the high relative abundance of HUPs compounds detected by FT-ICR MS. Riverine DOM displayed significantly spatial and seasonal differences. In the forest-dominated upstream reach, HUPs with high O/C and polyphenolic compounds, as well as microbial humic-like component were relatively abundant. However, the accumulation of CDOM content was limited due to higher flow. These highly oxygenated, aromatic and less hydrogenated DOM fractions would also be partially degraded during longitudinal transport process. The DOM pool midstream was mainly consisted of HUPs with low O/C compound and terrestrial humic-like component with higher molecular weight, unsaturation and humification degree. The increasing cropland and urban land uses downstream contributed an amount of heteroatomic molecules and labile compounds to DOM pool. During dry/cold seasons, highly unsaturated, aromatic and humified DOM fractions were preserved due to weaker dilution and photo-degradation. The abundance of these fractions would decrease with increasing river discharge and solar irradiance during wet and warm season, and meanwhile phytoplankton growth under warm temperature released some aliphatic and protein-like compounds. Our findings revealed that riverine DOM chemodiversity could be mainly caused by the hydrologic, meteorological conditions and anthropogenic activities throughout the whole basin, which improved our ability to predict the spatial and temporal dynamics and cycle of DOM in a larger river. In the future, we will extend the study region to the East China Sea to investigate biogeochemical cycling of DOM in a changing hydrology region, and further estimated specific terrestrial carbon injection into the ocean. Moreover, laboratory-based incubation experiments should be performed to provide insights on the overall reactivity of riverine molecules under bio- and photo-degradation processes based on discharge transport time.

Declaration of Competing Interest

We declare that we don't have any commercial or associative interest that represents a conflict of interest in connection with the submitted work.

Data availability

The authors do not have permission to share data.

Acknowledgements

This study was financially supported by the National Natural Science Foundation of China [Grant Nos. 41971286, 42277214, and 42207256], Major programs of the National Social Science Foundation of China [Grant No. 22&ZD136], Special Science and Technology Innovation Program for Carbon Peak and Carbon Neutralization of Jiangsu Province [Grant No. BE2022612], Postgraduate Research Innovation Project of

Jiangsu Province [Grant No. KYCX21_1338], China Scholarship Council [Grant No. 202006860045] and the Youth Top Talent funded by Nanjing Normal University. The Ion Cyclotron Resonance user facility at the National High Magnetic Field Laboratory at Florida State University is supported by the National Science Foundation Division of Materials Research and Division of Chemistry through DMR 16–44779, and the State of Florida. The author would like to thank J.H. Li, C. Wang and W. Y. Hao for their assistances with sampling.

Supplementary materials

Supplementary material associated with this article can be found, in the online version, at doi:10.1016/j.watres.2023.119812.

References

Allan, J.D., Wipfli, M.S., Caouette, J.P., Prussian, A., Rodgers, J., 2003. Influence of streamside vegetation on inputs of terrestrial invertebrates to salmonid food webs. Canad. J. Fisher. Aquatic Sci. 60 (3), 309–320.

Andrews, J.E., Greenaway, A.M., Dennis, P.F., 1998. Combined carbon isotope and C/N ratios as indicators of source and fate of organic matter in a poorly flushed, tropical estuary: hunts Bay, Kingston Harbour, Jamaica. Estuarine, Coast. Shelf Sci. 46 (5), 743–756.

Bai, Y., Su, R., Han, X., Zhang, C., Shi, X., 2015. Investigation of seasonal variability of CDOM fluorescence in the southern changjiang river estuary by EEM-PARAFAC. Acta Oceanologica Sinica 34 (10), 1–12.

Bao, H., Wu, Y., Zhang, J., 2015. Spatial and temporal variation of dissolved organic matter in the Changjiang: fluvial transport and flux estimation. J. Geophys. Res.: Biogeosci. 120 (9), 1870–1886.

Begum, M.S., Lee, M.H., Park, T.J., Lee, S.Y., Shin, K.H., Shin, H.S., Chen, M., Hur, J., 2022. Source tracking of dissolved organic nitrogen at the molecular level during storm events in an agricultural watershed. Sci. Total Environ. 810, 152183.

Behnke, M.I., McClelland, J.W., Tank, S.E., Kellerman, A.M., Holmes, R.M., Haghipour, N., Eglinton, T.I., Raymond, P.A., Suslova, A., Zhulidov, A.V., Gurtovaya, T., Zimov, N., Zimov, S., Mutter, E.A., Amos, E., Spencer, R.G.M., 2021. Pan-Arctic riverine dissolved organic matter: synchronous molecular stability, shifting sources and subsidies. Glob. Biogeochem. Cycles 35 (4), GB006871 e2020.

Berg, S.M., Whiting, Q.T., Herrli, J.A., Winkels, R., Wammer, K.H., Remucal, C.K., 2019. The role of dissolved organic matter composition in determining photochemical reactivity at the molecular level. Environ. Sci. Technol. 53 (20), 11725–11734.

Bianchi, T.S., Filley, T., Dria, K., Hatcher, P.G., 2004. Temporal variability in sources of dissolved organic carbon in the lower Mississippi River. Geochim. Cosmochim. Acta 68 (5), 959–967.

Chen, S., Du, Y., Das, P., Lamore, A.F., Dimova, N.T., Elliott, M., Broadbent, E.N., Roebuck Jr, J.A., Jaffé, R., Lu, Y., 2021. Agricultural land use changes stream dissolved organic matter via altering soil inputs to streams. Sci. Total Environ. 796, 148968.

Cleveland, C.C., Neff, J.C., Townsend, A.R., Hood, E., 2004. Composition, dynamics, and fate of leached dissolved organic matter in terrestrial ecosystems: results from a decomposition experiment. Ecosystems 7 (3), 175–285.

Corilo, Y., 2015. PetroOrg. Florida State University.

D`Andrilli, J., Cooper, W.T., Foreman, C.M., Marshall, A.G., 2015. An ultrahigh-resolution mass spectrometry index to estimate natural organic matter lability. Rapid Commun. Mass Spectrom.: RCM 29 (24), 2385–2401.

Derrien, M., Kim, M.S., Ock, G., Hong, S., Cho, J., Shin, K.H., Hur, J., 2018. Estimation of different source contributions to sediment organic matter in an agricultural-forested watershed using end member mixing analyses based on stable isotope ratios and fluorescence spectroscopy. Sci. Total Environ. 618, 569–578.

Dittmar, T., Koch, B., Hertkorn, N., Kattner, G., 2008. A simple and efficient method for the solid-phase extraction of dissolved organic matter (SPE-DOM) from seawater. Limnol. Oceanogr.: Methods 6 (6), 230–235.

Du, Y., Lu, Y., Roebuck Jr, J.A., Liu, D., Chen, F., Zeng, Q., Xiao, K., He, H., Liu, Z., Zhang, Y., Jaffé, R., 2021. Direct versus indirect effects of human activities on dissolved organic matter in highly impacted lakes. Sci. Total Environ. 752, 141839.

Figueroa, D., Capo, E., Lindh, M.V., Rowe, O.F., Paczkowska, J., Pinhassi, J., Andersson, A., 2021. Terrestrial dissolved organic matter inflow drives temporal dynamics of the bacterial community of a subarctic estuary (northern Baltic Sea). Environ. Microbiol. 23 (8), 4200–4213.

Gao, K., Zhou, Z., Yang, Y., 2010. Land use structure and its spatial autocorrelation analysis in the Yangtze River Basin (in Chinese with an English abstract). Resour. Environ. Yangtze Basin 19, 13–20.

GB/T11893, 1989. Water Quality—determination of total phosphorus—ammonium molybdate spectrophotometric method. (in Chinese).

Gomez-Saez, G.V., Niggemann, J., Dittmar, T., Pohlabeln, A.M., Lang, S.Q., Noowong, A., Pichler, T., Wörmer, L., Bühring, S.I., 2016. Molecular evidence for abiotic sulfurization of dissolved organic matter in marine shallow hydrothermal systems. Geochim. Cosmochim. Acta 190, 35–52.

Gong, C., Jiao, R., Yan, W., Yu, Q., Li, Q., Zhang, P., Li, Y., Wang, D., 2022. Enhanced chemodiversity, distinctive molecular signature and diurnal dynamics of dissolved organic matter in streams of two headwater catchments, Southeastern China. Water Res. 211, 118052.

Gonsior, M., Zwartjes, M., Cooper, W.J., Song, W., Ishida, K.P., Tseng, L.Y., Jeung, M.K., Rosso, D., Hertkorn, N., Schmitt-Kopplin, P., 2011. Molecular characterization of effluent organic matter identified by ultrahigh resolution mass spectrometry. Water Res. 45 (9), 2943–2953.

Hansell, D.A., Carlson, C.A., 2014. Biogeochemistry of Marine Dissolved Organic Matter. Academic Press.

Hedges, J.I., Keil, R.G., Benner, R., 1997. What happens to terrestrial organic matter in the ocean? Org. Geochem. 27 (5–6), 195–212.

Helms, J.R., Stubbins, A., Ritchie, J.D., Minor, E.C., Kieber, D.J., Mopper, K., 2008. Absorption spectral slopes and slope ratios as indicators of molecular weight, source, and photobleaching of chromophoric dissolved organic matter. Limnol. Oceanogr. 53 (3), 955–969.

HJ536, 2009, Quality-determination of ammonia nitrogen-salicylic acid spectrophotometry. (in Chinese).

HJ636, 2012, Water quality-determination of total nitrogen-alkaline potassium persulfate digestion UV spectrophotometric method. (in Chinese).

Johnston, S.E., Finlay, K., Spencer, R.G.M., Butman, D.E., Metz, M., Striegl, R., Bogard, M.J., 2022. Zooplankton release complex dissolved organic matter to aquatic environments. Biogeochemistry 157 (3), 313–325.

Kamjunke, N., Hertkorn, N., Harir, M., Schmitt-Kopplin, P., Griebler, C., Brauns, M., von Tümpling, W., Weitere, M., Herzsprung, P., 2019. Molecular change of dissolved organic matter and patterns of bacterial activity in a stream along a land-use gradient. Water Res. 164, 114919.

Kattner, G., Lobbes, J.M., Fitznar, H.P., Engbrodt, R., Nöthig, E.-M., Lara, R.J., 1999. Tracing dissolved organic substances and nutrients from the Lena River through Laptev Sea (Arctic). Mar Chem 65 (1–2), 25–39.

Kellerman, A.M., Guillemette, F., Podgorski, D.C., Aiken, G.R., Butler, K.D., Spencer, R.G. M., 2018. Unifying concepts linking dissolved organic matter composition to persistence in aquatic ecosystems. Environ. Sci. Technol. 52 (5), 2538–2548.

Kellerman, A.M., Kothawala, D.N., Dittmar, T., Tranvik, L.J., 2015. Persistence of dissolved organic matter in lakes related to its molecular characteristics. Nat. Geosci. 8 (6), 454–457.

Kellerman, A.M., Vonk, J., McColaugh, S., Podgorski, D.C., van Winden, E., Hawkings, J. R., Johnston, S.E., Humayun, M., Spencer, R.G.M., 2021. Molecular signatures of glacial dissolved organic matter from Svalbard and Greenland. Global Biogeochem. Cycles 35 (3), GB006709 e2020.

Koch, B.P., Dittmar, T., 2006. From mass to structure: an aromaticity index for high-resolution mass data of natural organic matter. Rapid Commun. Mass Spectrom. 20 (5), 926–932.

Kraus, T.E.C., Bergamaschi, B.A., Hernes, P.J., Doctor, D., Kendall, C., Downing, B.D., Losee, R.F., 2011. How reservoirs alter drinking water quality: organic matter sources, sinks, and transformations. Lake Reserv. Manag. 27 (3), 205–219.

Kurek, M.R., Stubbins, A., Drake, T.W., Dittmar, T., Moura, J.M., Holmes, R.M., Osterholz, H., Six, J., Wabakanghanzi, J.N., Dinga, B., Mitsuya, M., Spencer, R.G.M., 2022. Organic molecular signatures of the Congo River and comparison to the Amazon. Global Biogeochem. Cycles 36 (6), GB007301 e2022.

Lamb, A.L., Wilson, G.P., Leng, M.J., 2006. A review of coastal palaeoclimate and relative sea-level reconstructions using δ13C and C/N ratios in organic material. Earth-Sci. Rev. 75 (1–4), 29–57.

Lang, S.Q., Bernasconi, S.M., Früh-Green, G.L., 2012. Stable isotope analysis of organic carbon in small (μg C) samples and dissolved organic matter using a GasBench preparation device. Rapid Commun. Mass Spectrom. 26 (1), 9–16.

Lee, M.H., Lee, Y.K., Derrien, M., Choi, K., Shin, K.H., Jang, K.S., Hur, J., 2019. Evaluating the contributions of different organic matter sources to urban river water during a storm event via optical indices and molecular composition. Water Res. 165, 115006.

Leite, R.G., Araújo-Lima, C.A.R.M., Victória, R.L., Martinelli, L.A., 2002. Stable isotope analysis of energy sources for larvae of eight fish species from the Amazon floodplain. Ecol. Freshw Fish. 11 (1), 56–63.

Li, S., Fan, R., Luo, D., Xue, Q., Li, L., Yu, X., Huang, T., Yang, H., Huang, C., 2020. Variation in quantity and quality of rainwater dissolved organic matter (DOM) in a peri-urban region: implications for the effect of seasonal patterns on DOM fates. Atmos. Environ. 239, 117769.

Li, S., Fang, J., Zhu, X., Spencer, R.G.M., Álvarez-Salgado, X.A., Deng, Y., Huang, T., Yang, H., Huang, C., 2022. Properties of sediment dissolved organic matter respond to eutrophication and interact with bacterial communities in a plateau lake. Environ. Pollut. 301, 118996.

Liu, D., Pan, D., Bai, Y., He, X., Wang, D., Zhang, L., 2015. Variation of dissolved organic carbon transported by two Chinese rivers: the Changjiang River and Yellow River. Mar. Pollut. Bull. 100 (1), 60–69.

Marty, J., Planas, D., 2008. Comparison of methods to determine algal δ13C in freshwater. Limnol. Oceanogr.: Methods 6 (1), 51–63.

Medeiros, P.M., Seidel, M., Niggemann, J., Spencer, R.G.M., Hernes, P.J., Yager, P.L., Miller, W.L., Dittmar, T., Hansell, D.A., 2016. A novel molecular approach for tracing terrigenous dissolved organic matter into the deep ocean. Global Biogeochem. Cycles 30 (5), 689–699.

Medeiros, P.M., Seidel, M., Ward, N.D., Carpenter, E.J., Gomes, H.R., Niggemann, J., Krusche, A.V., Richey, J.E., Yager, P.L., Dittmar, T., 2015. Fate of the Amazon River dissolved organic matter in the tropical Atlantic Ocean. Global Biogeochem. Cycles 29 (5), 677–690.

Meng, L., Zhao, Z., Lu, L., Zhou, J., Luo, D., Fan, R., Li, S., Jiang, Q., Huang, T., Yang, H., Huang, C., 2021. Source identification of particulate organic carbon using stable isotopes and n-alkanes: modeling and application. Water Res. 197, 117083.

Miranda, M.L., Osterholz, H., Giebel, H.A., Bruhnke, P., Dittmar, T., Zielinski, O., 2020. Impact of UV radiation on DOM transformation on molecular level using FT-ICR-MS and PARAFAC. Spectrochim Acta A Mol Biomol Spectrosc 230, 118027.

Murphy, K.R., Butler, K.D., Spencer, R.G.M., Stedmon, C.A., Boehme, J.R., Aiken, G.R., 2010. Measurement of dissolved organic matter fluorescence in aquatic environments: an lnterlaboratory comparison. Environ. Sci. Technol. 44 (24), 9405–9412.

Murphy, K.R., Stedmon, C.A., Wenig, P., Bro, R., 2014. OpenFluor–an online spectral library of auto-fluorescence by organic compounds in the environment. Anal. Methods 6 (3), 658–661.

Nkoue Ndondo, G.R., Probst, J.-L., Ndjama, J., Ndam Ngoupayou, J.R., Boeglin, J.-L., Takem, G.E., Brunet, F., Mortatti, J., Gauthier-Lafaye, F., Braun, J.-J., Ekodeck, G.E., 2021. Stable carbon isotopes δ13C as a proxy for characterizing carbon sources and processes in a small tropical headwater catchment: nsimi, Cameroon. Aquatic Geochem. 27 (1), 1–30.

Osburn, C.L., Boyd, T.J., Montgomery, M.T., Bianchi, T.S., Coffin, R.B., Paerl, H.W., 2016. Optical proxies for terrestrial dissolved organic matter in estuaries and coastal waters. Front. Mar. Sci. 2, 127.

Pang, Y., Wang, K., Sun, Y., Zhou, Y., Yang, S., Li, Y., He, C., Shi, Q., He, D., 2021. Linking the unique molecular complexity of dissolved organic matter to flood period in the Yangtze River mainstream. Sci. Total Environ. 764, 142803.

Paul, D., Skrzypek, G., Fórizs, I., 2007. Normalization of measured stable isotopic compositions to isotope reference scales – a review. Rapid Commun. Mass Spectrom. 21, 3006–3014.

Raymond, P.A., Spencer, R.G., 2015. Riverine DOM, Biogeochemistry of Marine Dissolved Organic Matter. Elsevier, pp. 509–533.

Remington, S., Krusche, A., Richey, J., 2011. Effects of DOM photochemistry on bacterial metabolism and CO2 evasion during falling water in a humic and a whitewater river in the Brazilian Amazon. Biogeochemistry 105 (1–3), 185–200.

Roth, V.N., Lange, M., Simon, C., Hertkorn, N., Bucher, S., Goodall, T., Griffiths, R.I., Mellado-Vázquez, P.G., Mommer, L., Oram, N.J., Weigelt, A., Dittmar, T., Gleixner, G., 2019. Persistence of dissolved organic matter explained by molecular changes during its passage through soil. Nat. Geosci. 12 (9), 755–761.

Schmitt-Kopplin, P., Gelencser, A., Dabek-Zlotorzynska, E., Kiss, G., Hertkorn, N., Harir, M., Hong, Y., Gebefügi, I., 2010. Analysis of the unresolved organic fraction in atmospheric aerosols with ultrahigh-resolution mass spectrometry and nuclear magnetic resonance spectroscopy: organosulfates as photochemical smog constituents. Anal. Chem. 82 (19), 8017–8026.

Smith, D.F., Podgorski, D.C., Rodgers, R.P., Blakney, G.T., Hendrickson, C.L., 2018. 21 tesla FT-ICR mass spectrometer for ultrahigh-resolution analysis of complex organic mixtures. Anal. Chem. 90 (3), 2041–2047.

Spencer, R.G.M., Guo, W., Raymond, P.A., Dittmar, T., Hood, E., Fellman, J., Stubbins, A., 2014. Source and biolability of ancient dissolved organic matter in glacier and lake ecosystems on the Tibetan Plateau. Geochim. Cosmochim. Acta 142 (1), 64–74.

Spencer, R.G.M., Kellerman, A.M., Podgorski, D.C., Macedo, M.N., Jankowski, K., Nunes, D., Neill, C., 2019. Identifying the molecular signatures of agricultural expansion in Amazonian headwater streams. J. Geophys. Res.: Biogeosci. 124 (6), 1637–1650.

Spencer, R.G.M., Stubbins, A., Hernes, P.J., Baker, A., Mopper, K., Aufdenkampe, A.K., Dyda, R.Y., Mwamba, V.L., Mangangu, A.M., Wabakanghanzi, J.N., Six, J., 2009. Photochemical degradation of dissolved organic matter and dissolved lignin phenols from the Congo River. J. Geophys. Res. 114 (G3). G3.

Stedmon, C.A., Bro, R., 2008. Characterizing dissolved organic matter fluorescence with parallel factor analysis: a tutorial. Limnol. Oceanogr.: Methods 6 (11), 572–579.

Stock, B.C., Jackson, A.L., Ward, E.J., Parnell, A.C., Phillips, D.L., Semmens, B.X., 2018. Analyzing mixing systems using a new generation of Bayesian tracer mixing models. PeerJ 6, e5096.

Stubbins, A., Spencer, R.G.M., Chen, H., Hatcher, P.G., Mopper, K., Hernes, P.J., Mwamba, V.L., Mangangu, A.M., Wabakanghanzi, J.N., Six, J., 2010. Illuminated darkness: molecular signatures of Congo River dissolved organic matter and its photochemical alteration as revealed by ultrahigh precision mass spectrometry. Limnol. Oceanogr. 55 (4), 1467–1477.

Sun, X., Fan, D., Cheng, P., Hu, L., Sun, X., Guo, Z., Yang, Z., 2021. Source, transport and fate of terrestrial organic carbon from Yangtze River during a large flood event: insights from multiple-isotopes (δ13C, δ15N, Δ14C) and geochemical tracers. Geochim. Cosmochim. Acta 308, 217–236.

Tang, J., Wang, W., Yang, L., Qiu, Q., Lin, M., Cao, C., Li, X., 2020. Seasonal variation and ecological risk assessment of dissolved organic matter in a peri-urban critical zone observatory watershed. Sci. Total Environ. 707, 136093.

Vaughn, D.R., Kellerman, A.M., Wickland, K.P., Striegl, R.G., Podgorski, D.C., Hawkings, J.R., Nienhuis, J.H., Dornblaser, M.M., Stets, E.G., Spencer, R.G.M., 2021. Anthropogenic landcover impacts fluvial dissolved organic matter composition in the Upper Mississippi River Basin. Biogeochemistry, pp. 1–25.

Waiser, M.J., Robarts, R.D., 2004. Photodegradation of DOC in a shallow prairie wetland: evidence from seasonal changes in DOC optical properties and chemical characteristics. Biogeochemistry 69 (2), 263–284.

Wang, B., Wu, L., 2021. Numerical study on the massive outbreak of the Ulva prolifera Green tides in the southwestern Yellow Sea in 2021. J .Mar. Sci. Eng. 9 (11), 1167.

Wang, J., Gu, B., Huang, J., Han, X., Lin, G., Zheng, F., Li, Y., 2014. Terrestrial contributions to the aquatic food web in the middle Yangtze River. PLoS ONE 9 (7), e102473.

Wang, K., Li, P., He, C., Shi, Q., He, D., 2021. Hydrologic heterogeneity induced variability of dissolved organic matter chemistry among tributaries of the Three Gorges Reservoir. Water Res. 201, 117358.

Wen, Z., Shang, Y., Lyu, L., Liu, G., Hou, J., He, C., Shi, Q., He, D., Song, K., 2021. Sources and composition of riverine dissolved organic matter to marginal seas from mainland China. J. Hydrol. (Amst.) 603, 127152.

Wu, Y., Zhang, J., Liu, S.M., Zhang, Z.F., Yao, Q.Z., Hong, G.H., Cooper, L., 2007. Sources and distribution of carbon within the Yangtze River system. Estuar. Coast. Shelf Sci. 71 (1–2), 13–25.

Zhai, W., Dai, M., Guo, X., 2007. Carbonate system and CO2 degassing fluxes in the inner estuary of Changjiang (Yangtze) River, China. Mar. Chem. 107 (3), 342–356.

Zhang, Y., Zhou, L., Zhou, Y., Zhang, L., Yao, X., Shi, K., Jeppesen, E., Yu, Q., Zhu, W., 2021. Chromophoric dissolved organic matter in inland waters: present knowledge and future challenges. Sci. Total Environ. 759, 143550.

Zhao, L., Gao, L., Guo, L., 2021a. Seasonal variations in molecular size of chromophoric dissolved organic matter from the lower Changjiang (Yangtze) River. J. Geophys. Res.: Biogeosci. 126 (8), e2020.

Zhao, Z., Huang, C., Meng, L., Lu, L., Wu, Y., Fan, R., Li, S., Sui, Z., Huang, T., Huang, C., Yang, H., Zhang, L., 2021b. Eutrophication and lakes dynamic conditions control the endogenous and terrestrial POC observed by remote sensing: modeling and application. Ecol. Indic. 129, 107907.

Zhou, C., Liu, Y., Liu, C., Liu, Y., Tfaily, M.M., 2019. Compositional changes of dissolved organic carbon during its dynamic desorption from hyporheic zone sediments. Sci. Total Environ. 658, 16–23.

Zhou, Y., Guo, H., Lu, H., Mao, R., Zheng, H., Wang, J., 2015. Analytical methods and application of stable isotopes in dissolved organic carbon and inorganic carbon in groundwater. Rapid Commun. Mass Spectrom. 29 (19), 1827–1835.

Zhou, Y., Yao, X., Zhou, L., Zhao, Z., Wang, X., Jang, K.S., Tian, W., Zhang, Y., Podgorski, D.C., Spencer, R.G.M., Kothawala, D.N., Jeppesen, E., Wu, F., 2021. How hydrology and anthropogenic activity influence the molecular composition and export of dissolved organic matter: observations along a large river continuum. Limnol. Oceanogr. 66 (5), 1730–1742.